AGU ADVANCING EARTH AND SPACE SCIENCE

Earth's Future

Key Points:
- Biomass turnover time (τ) and net primary production (NPP) generally have opposite trends in tropical forest
- Decreasing NPP and increasing τ are associated with rainfall >2,000 mm·y^{-1}, while opposite trends are associated with rainfall <2,000 mm·y^{-1}
- Decreasing NPP and increasing τ mainly depend on temperature and vapor pressure deficit, while the opposite trends on radiation and rainfall

Supporting Information:
- Supporting Information S1

Correspondence to:
W. Li,
wli2019@tsinghua.edu.cn

Changes in Biomass Turnover Times in Tropical Forests and Their Environmental Drivers From 2001 to 2012

Jingmeng Wang[1,2] , Wei Li[1,2] , Philippe Ciais[3], Ashley Ballantyne[3,4], Daniel Goll[3,5] , Xiaomeng Huang[1] , Zhe Zhao[1,2], and Lei Zhu[1,2]

[1]Ministry of Education Key Laboratory for Earth System Modeling, Department of Earth System Science, Tsinghua University, Beijing, China, [2]Joint Center for Global Change Studies, Beijing, China, [3]Laboratoire des Sciences du Climat et de l'Environnement, LSCE/IPSL, CEA-CNRS-UVSQ, Université Paris-Saclay, Gif-sur-Yvette, France, [4]Department of Ecosystem and Conservation Sciences, University of Montana, Missoula, MT, USA, [5]Department of Geography, University of Augsburg, Augsburg, Germany

Abstract Tropical forests store about 70% of the total living biomass on land and yet very little is known about changes in this vital carbon reservoir. Changes in their biomass stock, determined by changes in carbon input (i.e., net primary production [NPP]) and carbon turnover time (τ), are critical to the global carbon sink. In this study, we calculated transient τ in tropical forest biomass using satellite-based biomass and moderate-resolution imaging spectroradiometer (MODIS) NPP and analyzed the trends of τ and NPP from 2001 to 2012. Results show that τ and NPP generally have opposite trends across the tropics. Increasing NPP and decreasing τ ("N+T−") mainly distribute in central Africa and the northeast region of South America, while decreasing NPP and increasing τ ("N−T+") prevail in Southeast Asia and western Amazon forests. Most of the N+T− tropical forest areas are associated with mean annual precipitation (MAP) below 2,000 mm·y^{-1} and most N−T+ tropical forests with MAP above 2,000 mm·y^{-1}. The τ and NPP trends in the N+T− region are statistically associated with radiation, precipitation and vapor pressure deficit (VPD), while the τ and NPP trends in the N−T+ region are mainly associated with temperature and VPD. Our results inherit the uncertainties from the satellite-based datasets and largely depend on the carbon use efficiency from MODIS. We thus systematically assessed the robustness of the findings. Our study reveals regional patterns and potential drivers of biomass turnover time and NPP changes and provides valuable insights into the tropical forest carbon dynamics.

Plain Language Summary Tropical forest biomass and its response to climate change is of great importance to global carbon cycle. How carbon stock of tropical forest biomass will change depends on changes in carbon input (i.e., net primary production [NPP]) and how long carbon will stay in the biomass (i.e., turnover time [τ]). Higher NPP and longer τ will persistently increase tropical forest biomass, and vice versa. In this study, we used satellite-based biomass and NPP dataset to calculate τ. We found NPP and τ generally have opposite trends during 2001–2012. In regions with mean annual precipitation >2,000 mm·y^{-1}, there are mainly increasing NPP and decreasing τ, affected by radiation, precipitation and vapor pressure deficit [VPD]. In contrast, regions with mean annual precipitation <2,000 mm·y^{-1} is dominated by decreasing NPP and increasing τ, associated with the changes of temperature and VPD. Results from this study help us understand the processes and predict the future changes in the tropical forest carbon dynamics.

1. Introduction

Tropical forests play a key role in the global carbon (C) cycle and the climate system (Keenan et al., 2015). They contain 70% of the global live biomass, that is, about 250 Pg carbon (Pg C) (Baccini et al., 2017; Liu et al., 2015; Pan et al., 2011; Saatchi et al., 2011). Because of its large carbon stock as well as high sensitivity to climate variability (Cox et al., 2013; Seddon et al., 2016) and disturbances (Baccini et al., 2017), the future dynamics of tropical forest biomass could result in a large amount of carbon sequestered from or released to the atmosphere (Mitchard, 2018). The response of the biomass carbon stocks in tropical forests to climate change and anthropogenic land use disturbances thus contributes to feedbacks of the carbon cycle on global atmospheric carbon dioxide (CO_2) concentration.

Tropical forest C dynamics are tightly coupled to energy and water exchange between the biosphere and atmosphere (Bonan, 2008). Earlier studies suggested that tropical forest productivity could be limited more by solar radiation than by temperature and water (Graham et al., 2003; Nemani, 2003; Seddon et al., 2016). Recent work suggests that temperature is also important in wet forests that operate close to a temperature optimum for their productivity (Corlett, 2011; Huang et al., 2019). Droughts induced by high temperature and low precipitation may increase tree mortality and cause a legacy carbon source for several years after the drought, as shown for the Amazon (Brienen et al., 2015; Phillips et al., 2009; Yang et al., 2018). However, much less is known about the response of pantropical forest biomass to climate variations because of diverse physiological processes involved.

The complex physiological processes controlling biomass carbon stock dynamics can be grouped into controls on carbon input (i.e., net primary production [NPP]) (W. Wang et al., 2011; Zhou et al., 2018) and controls on how fast carbon will be released from biomass pools (defined as carbon turnover time [τ]) (De Kauwe et al., 2014; Koven et al., 2015). As two major components, NPP and τ regulate the total biomass carbon (TBC, i.e., sum of the aboveground and belowground biomass) through the equilibrium carbon storage capacity (C_{cap}), which equals to NPP multiplied by τ (Luo et al., 2017; Xia et al., 2013). C_{cap} represents the maximum capability of a carbon pool to sequestrate carbon based on instantaneous environmental forcing (Luo et al., 2017). TBC will always converge towards C_{cap} (Luo et al., 2017). When C_{cap} is dynamic with a changing environment, the tendency of TBC will adjust correspondingly. In an ideal steady state, TBC approximates to C_{cap} (fluctuates tightly around C_{cap}) and reaches its equilibrium (L. Jiang et al., 2017; Luo et al., 2017). Therefore, the changes in TBC are largely dependent on the trends of τ and NPP, which are impacted by conditions of heat, water and energy (Seddon et al., 2016; Wu et al., 2018).

The climate responses of NPP and τ may contribute differently to biomass change. For example, higher temperature may stimulate NPP before reaching the optimum temperature (Huang et al., 2019; Raich et al., 2006) but may also increase mortality and accelerate τ (Mitchard, 2018; Park Williams et al., 2013), leading to different effects on carbon stock. Brienen et al. (2015) also showed that although forest productivity in the Amazon slightly increased since 1980s, carbon stock decreased because of a faster increase in mortality (indicating lower τ). In addition, climate, soil fertility conditions and forest species and their traits are unevenly distributed within tropical forests (Anderegg et al., 2018; Guan et al., 2015). Therefore, different patterns of climate change impacts on biomass would be expected in different regions of the tropics. For example, Guan et al. (2015) pointed out that forest gross primary productivity (GPP) is higher in the wet season than in the dry season in central Africa, while the opposite was true in the Amazon forest north of the equator. Unlike productivity, however, there is no direct observation of turnover time. Carvalhais et al. (2014) and Wu et al. (2018) analyzed the spatial patterns of turnover time assuming steady state, where turnover time is calculated from the carbon pool stock divided by the input flux (i.e., mass/flux). But real ecosystems are rarely in equilibrium, and how turnover time changes over time remains unclear.

In this study, we deduced transient turnover time of tropical forest from satellite-derived annual estimates of biomass stock and NPP from 2001 to 2012. We examined changes of τ and NPP in different tropical regions and further explored how climate variations (temperature, precipitation, radiation and vapor pressure deficit [VPD]) contributed to different temporal trends of τ or NPP across different regions in the tropical forest along mean annual precipitation (MAP) gradient.

2. Materials and Methods

2.1. MODIS NPP Data

We used forest NPP from the 1 km MOD17A3 product, a light use efficiency model applied to moderate-resolution imaging spectroradiometer (MODIS) observations of FPAR, the fraction of absorbed photosynthetically active sunlight (Zhao et al., 2005). Based on MODIS land cover map (MOD12C1, 0.05°) (Friedl et al., 2010), only grid cells classified as forest in all years during 2001–2012 are used to build the forest mask. The original 1 km NPP dataset was resampled at the resolution of MOD12C1 data (0.05°), to separate forest and non-forest NPP. The multiyear average and standard deviation (1-σ, the same below) of total NPP in the tropical forest biome was 18.7 ± 0.3 PgC·y^{-1} (Figure S1c), while the tropical non-forest NPP was 9.3 ± 0.3

PgC·y^{-1}. Forest NPP and non-forest NPP were further resampled at 0.25° resolution to match the resolution of biomass data used in this study (see Section 2.2).

2.2. Tropical Forest Biomass Data

Aboveground biomass carbon (ABC) in tropical forests (23.5°N to 23.5°S) during 2001–2012 was extracted from the global ABC dataset of Liu et al. (2015). The biomass dataset from Liu et al. (2015) was derived from harmonized X-band vegetation optical depth (VOD) retrievals based on passive microwave satellite sensors (Liu et al., 2011, 2015). In this study, ABC was converted to TBC by using biome-mean conversion factors (TBC/ABC ratios) from Liu et al. (2015), with a value of 1.26 for tropical forest. Based on the assumption that the biomass carbon turnover time of non-forest vegetation (mostly shrub and grass) was around one year (Lauenroth & Adler, 2008), non-forest TBC approximates annual non-forest NPP (Erb et al., 2016). Therefore, we subtract annual non-forest NPP from TBC in each 0.25° grid cell in order to derive pure forest TBC from the coarse resolution (0.25°) TBC map. The multiyear averaged total TBC in our study region was 234.4 ± 2.1 PgC, including 225.2 ± 2.3 PgC for forest (Figure S2a) and 9.2 ± 0.3 PgC for non-forest.

2.3. Fire Mask and Climatic Datasets

Tropical forest is subject to both natural and anthropogenic fire (Mitchard, 2018). Forest fires cause large carbon emission and may have long-term effects, such as changes in age composition, degradation and succession (Brando et al., 2019; Deklerck et al., 2019; Pellegrini et al., 2017; Pugh et al., 2019). Fire disturbance may change the response of forest TBC to climatic factors because of its strong effects on forest carbon cycle (Pellegrini et al., 2017; Pugh et al., 2019). In order to exclude the impacts of fire, we use the burned area product (Fire_CCI) from the European Space Agency (ESA) (Chuvieco et al., 2012). We calculated the burned area fraction at 0.25° for MODIS NPP, and only grid cells with more than 90% of area without fire disturbance in all years during the study period were analyzed for turnover times (Figure S3). Because we separated forest NPP from non-forest NPP and only analyzed grids which are persistently defined as forest, the impacts of land use change were largely excluded. In the tropical forest that was not disturbed by land use change and fire, we further attributed changes of turnover time and NPP to changes of temperature, precipitation, radiation and VPD. We used monthly temperature and precipitation data from Climate Research Unit (CRU TS version 4.02, http://www.cru.uea.ac.uk/cru/data/hrg/) and shortwave radiation data from the BESS dataset based on MODIS data (Ryu et al., 2018). To obtain VPD, we used surface pressure, 2-m air temperature and specific humidity from blended datasets of Climatic Research Unit and Japanese Meteorological Agency reanalysis (CRU JRA V1.1, University of East Anglia Climatic Research Unit; Harris (2019)). VPD was calculated using the R package "bigleaf" (Knauer et al., 2018). The spatial resolution is 0.25° for radiation data and 0.5° for temperature, precipitation and VPD data. The temporal resolution of climatic data was integrated into annual scale. Temperature, precipitation and VPD data were resampled at 0.25° resolution to match the resolution of NPP and TBC.

2.4. Data Analysis

Based on annual forest TBC and NPP, the steady state carbon turnover time (τ, y) is defined as the ratio between carbon stock and net carbon output flux (Zhou et al., 2018):

$$\tau = \frac{\text{TBC}}{\text{NPP} - \text{dTBC}} \tag{1}$$

where, dTBC (kgC·m^{-2} y^{-1}) is the annual change in TBC. Net output flux of TBC is defined as the difference between NPP and changes of TBC (i.e., NPP−dTBC, kgC·m^{-2}· y^{-1}). Because we excluded the impacts of fire and land cover change, carbon output flux includes processes like litter fall, mortality, VOCs (volatile organic compounds) emission and disturbances like drought and herbivory. In some grid cells, negative values of τ were derived because NPP < dTBC. However, these grid cells only account for 0.5% of our study region, and we thus masked them in the following analyses. C_{cap} can be calculated by

$$C_{\text{cap}} = \text{NPP} \cdot \tau \qquad (2)$$

Because TBC in tropical forests is not in equilibrium, τ and C_{cap} also change in response to changing climate, and their multiyear mean values are shown inFigures S4 andS5, respectively. 3-year moving averages of τ, NPP and the climatic factors were used for the subsequent analyses to avoid the impacts of anomalous years. We calculated linear trends of forest τ and NPP from 2001 to 2012 for each grid cell. The significant trends ($p < 0.1$) of τ and NPP in each grid cell were used to define subregions in our study (see Section 3.1). We also did a Mann-Kendall test to verify the linear trends (see Section 4.2) by package "Kendall" (version 2.2) in R. We further divided our study period into two-half segments (i.e., the period before 2006 and the period after 2006), and tested whether the mean values of τ or NPP during the latter segment are significantly different from the mean values during the former one. Relative trends (absolute trend divided by average) and interannual variability (IAV, coefficient of temporal variation) of detrended NPP, τ and biomass were also calculated to analyze their temporal variations during 2001–2012 (see Section 4.2).

To analyze how climatic factors impact changes of τ and NPP, partial correlations of climatic factors with τ or NPP were calculated. Then, we fitted a multiple linear regression model with the 3-year moving average data in each grid cell (Equation 3).

$$y = \beta_0 + \beta_{\text{Tmp.}} x_{\text{Tmp.}} + \beta_{\text{Pre.}} x_{\text{Pre.}} + \beta_{\text{Rad.}} x_{\text{Rad.}} + \beta_{\text{VPD}} x_{\text{VPD}} + Resi. \qquad (3)$$

where, y is τ or NPP in each year; explanatory variable $x_{\text{Tmp.}}$, $x_{\text{Pre.}}$, $x_{\text{Rad.}}$ and x_{VPD} is yearly temperature, precipitation, shortwave radiation and VPD, respectively. $\beta_{\text{Tmp.}}$, $\beta_{\text{Pre.}}$, $\beta_{\text{Rad.}}$ and β_{VPD} represent temporal sensitivities of τ or NPP to changes of temperature, precipitation, shortwave radiation and VPD; $Resi.$ represents the residual.

Furthermore, we calculated the linear trends of temperature $\left(\frac{dx_{\text{Tmp.}}}{dt}\right)$, precipitation $\left(\frac{dx_{\text{Pre.}}}{dt}\right)$, radiation $\left(\frac{dx_{\text{Rad.}}}{dt}\right)$ and VPD $\left(\frac{dx_{\text{VPD}}}{dt}\right)$ in order to further quantify the contributions of climatic factors to the trends of τ or NPP $\left(\frac{dy}{dt}\right.$ in Equation 4$\left.\right)$. Thus, $\frac{dy}{dt}$ can be expressed as $\beta_i \frac{dx_i}{dt}$ (i = Tmp., Pre., Rad. and VPD) and the trend of residual $\left(\frac{dResi.}{dt}\right)$ in Equation 4.

$$\frac{dy}{dt} = \beta_{\text{Tmp.}} \frac{dx_{\text{Tmp.}}}{dt} + \beta_{\text{Pre.}} \frac{dx_{\text{Pre.}}}{dt} + \beta_{\text{Rad.}} \frac{dx_{\text{Rad.}}}{dt} + \beta_{\text{VPD}} \frac{dx_{\text{VPD}}}{dt} + \frac{dResi.}{dt} \qquad (4)$$

2.5. Other NPP Datasets for Validation

To evaluate the robustness of the results based on MODIS NPP, we also tested NPP from GIMMS (Smith et al., 2016), and NPP derived from GPP estimates from BESS (C. Jiang & Ryu, 2016) and the updated P-model from Stocker et al. (2019) (Stocker19, hereafter). Brief description of these NPP datasets can be found in Table S1. The GIMMS NPP dataset was mainly based on the remote sensing products (i.e., LAI3g and FPAR3g) from Global Inventory Modeling and Mapping Studies (GIMMS) and used the same light use efficiency algorithm as MODIS NPP (Smith et al., 2016; Zhu et al., 2013). The original datasets of BESS and Stocker19 are GPP instead of NPP, and we multiplied GPP by the carbon use efficiency (CUE = NPP/GPP) in each year from MOD17A3 product (mean CUE is 0.42 ± 0.08 across the tropical forest, Figure S6) to convert GPP to NPP (more details in Text S1). In BESS, GPP was calculated based on MODIS leaf area index (LAI) and a simplified process-based model including radiation transfer, canopy photosynthesis and evapotranspiration (C. Jiang & Ryu, 2016; Ryu et al., 2011). In Stocker et al. (2019), GPP was calculated from a leaf scale photosynthesis model driven by climate variables and assuming coordinated photosynthesis (P-model) (H. Wang et al., 2017) with MODIS FPAR, accounting for soil moisture stress on GPP (Stocker et al., 2019).

NPP derived from the GPP of BESS and Stocker19 cover the time period of the MODIS NPP product (2001–2012), but GIMMS NPP only covers 2001 to 2011. The resolution of NPP from GIMMS, BESS and Stocker19 is 1°, 0.5°, and 0.5°, respectively, so it is not possible to separate forest NPP from non-forest NPP directly at a finer resolution. We therefore used the ratio between forest NPP and non-forest NPP from MODIS NPP data in each corresponding grid cell to derive forest NPP map from the other three NPP datasets. Total NPP in the tropical forest was 14.1 ± 0.2, 14.4 ± 0.2, and 12.2 ± 0.2 PgC·y^{-1} based on GIMMS, BESS and Stocker19, respectively, which is lower than MODIS NPP (i.e., 18.7 ± 0.3 PgC·y^{-1}, Figure S1c). In addition, the spatial patterns of NPP from these three datasets were different from MODIS NPP, especially in the dry tropical forests (Figure S1). For the analysis based on NPP from GIMMS, BESS and Stocker19, gridded radiation data (0.25°) were resampled at 0.5° resolution.

To assess the satellite based NPP and τ trends, we collected site-level field observations from ForestPlots.net (http://www.forestplots.net/) repository (Lopez-Gonzalez et al., 2011): NPP and carbon loss in tropical Africa (Hubau et al., 2020); NPP, carbon loss and biomass in Amazon (Brienen et al., 2015) within our study region. Trends from satellite-based data were then compared against the trends from field data (see Section 4.3 and Text S2).

3. Results

3.1. Trends of Turnover Time and NPP During 2001–2012

Trends of τ and MODIS NPP show generally opposite spatial patterns (Figures 1a and 1b and Figures S7 and S8). τ decreased along the Atlantic coast (in central Africa and northeastern South America) but increased along the Pacific coast (Southeast Asia and western Amazon) as shown in Figure 1a. On the contrary, MODIS NPP shows an increasing trend in regions near the Atlantic coast but decreasing along the Pacific coast (Figure 1b). Because τ and NPP jointly determine the C_{cap} (Equation 2) which further controls TBC, opposite trends of τ and NPP result in a nonsignificant C_{cap} trend (Figure S9) and a weak TBC trend (Figure S2) in most regions. These results suggest a strong spatial covariance between NPP and τ.

There were 70.4% grid cells (0.25°) with significant trends ($p < 0.1$) of either τ or NPP, and 46.1% grid cells with significant trends for both τ and NPP (Table S2). Based on grid cells with significant trends of both τ and NPP, we divided the study area into four subregions (Figure 1c and Table S2): (1) increasing NPP and increasing τ (N+T+), (2) decreasing NPP and increasing τ (N−T+), (3) increasing NPP and decreasing τ (N+T−), and (4) decreasing NPP and decreasing τ (N−T−). An increasing input flux and increasing turnover time (i.e., decreasing output flux) in the N+T+ subregion would sequester more carbon by increasing C_{cap}, while grid cells in N−T− regions are losing carbon from biomass pools. The total area of these grid cells is very small across tropical forest, representing only 0.4% and 1.2% of all tropical forests, respectively (Table S2). The few N+T+ grid cells are found mainly in Africa and the few N−T− ones are in South America and Southeast Asia (Figure 1c). The N−T+ and N+T− subregions, on the other hand, cover most parts of tropical forests (blue and green colors in Figure 1c), which could be expected from the covariance of NPP and τ trends in Figures 1a and 1b. The future change in forest C_{cap} and TBC in these two subregions remains uncertain since most grid cells have opposite trends of τ and NPP (Figures 1a and 1b). Whether future C_{cap} and TBC will steadily increase or decrease largely depends on the trade-off between the trends of τ and NPP. Thus, we will mainly focus on the two subregions (N−T+ and N+T−) hereafter.

We further analyzed grid cells in these two subregions in relation with spatial patterns of mean annual precipitation (MAP, Figure S10). After plotting the frequency distribution of the N−T+ and N+T− subregions along MAP gradient (the inset plot in Figure 1c), we found a MAP threshold at about 2,000 mm·y^{-1} that separates these two subregions. The N+T− grid cells with MAP <2,000 mm·y^{-1} are mainly in central Africa (i.e., rainforests in DRC) while the fewer N+T− grid-cells with MAP >2,000 mm·y^{-1} are in the central Amazon north of the equator and in the Guyana shield (Figure 1c and Figure S10). Most N−T+ grid cells with MAP >2,000 mm·y^{-1} are in western Amazon and Southeast Asia and the fewer ones with MAP <2,000 mm·y^{-1} are around the border between Brazil and Peru (Figure 1c and Figure S10).
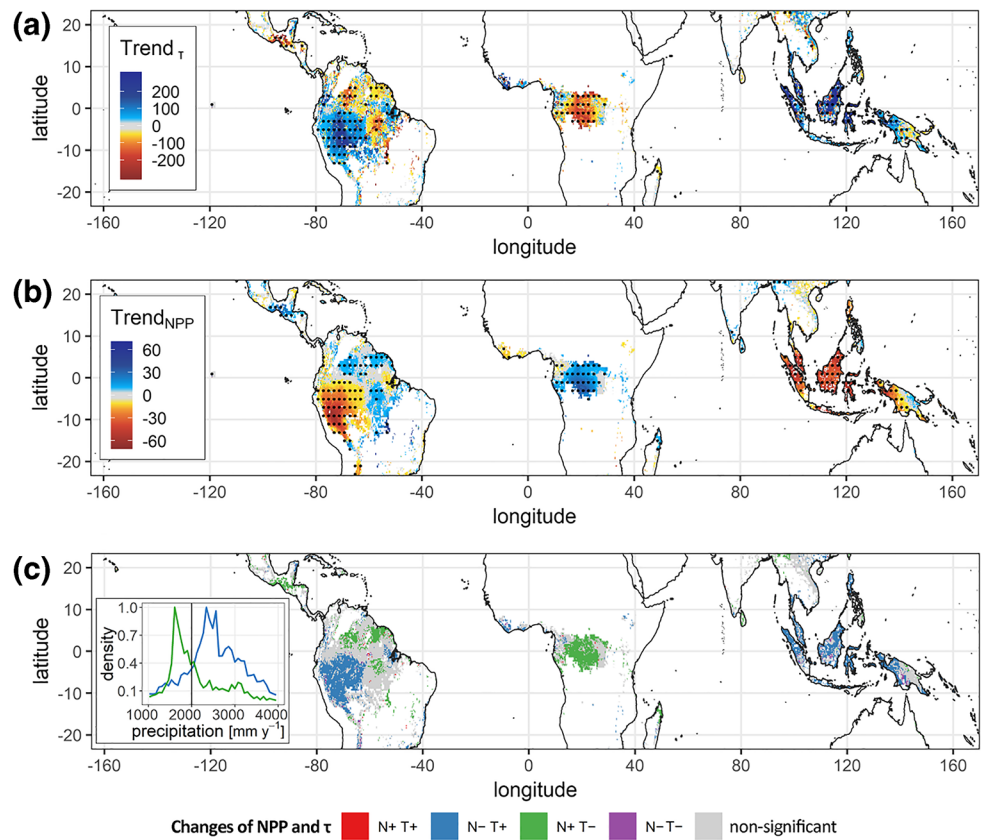
Figure 1. Trends of turnover time (τ) and NPP during 2001–2012 and division of four subregions. Panels (a and b) show trends of τ (day·y^{-1}) and NPP (gC·m^{-2} y^{-2}), respectively, with dots indicating the significant trends ($p < 0.1$). The division of four subregions in panel c was based on the significant trends in panels (a and b) ("N" and "T" refer to NPP and τ). Standardized frequency (the range of density was stretched into 0 to 1) of grid cell number with colors corresponding to N+T− and N−T+ subregions along the MAP gradient is embedded in panel (c). MAP, mean annual precipitation; NPP, net primary production.

3.2. Partial Correlations Between Climatic Variables and Turnover Time or NPP

Partial correlations between annual τ or NPP time series and time series of temperature, precipitation, radiation and VPD were calculated as described in Section 2.4. Spatial distributions of (temporal) partial correlation coefficients between each climatic factor and τ or NPP are shown in Figures S11 and S12.

Figure 2 shows heat maps of (temporal) partial correlation coefficients between each climatic factor and τ or NPP in the N−T+ and N+T− subregions along the MAP gradient. In grid cells with MAP <2,000 mm·y^{-1}, about half grid cells show a positive correlation τ and temperature, and the other half show a negative correlation, but when MAP exceeds 2,000 mm·y^{-1}, τ is mainly negatively correlated with temperature (Figure 2a). Negative partial correlation between τ and precipitation is dominant in regions with MAP <2,000 mm·y^{-1} (Figure 2b). Partial correlation coefficients between τ and precipitation gather in strong negative values around MAP of 2,000 mm·y^{-1}, and become weak when MAP >2,400 mm·y^{-1} (Figure 2b). The partial correlations between τ and radiation are mainly negative in regions with MAP <2,000 mm·y^{-1} and weak in regions with MAP >2,000 mm·y^{-1} (Figure 2c). The correlations of τ with VPD are rather symmetrical to those with temperature, with mainly positive and fewer negative values for MAP <2,000 mm·y^{-1} (Figure 2d) and mainly positive values for MAP >2,000 mm·y^{-1} (Figure 2d).

In summary, for most of the drier grid cells near the lower range of tropical MAP (<2,000 mm·y^{-1}), partial correlations between τ and radiation tend to be more negative (from −0.6 to −1.0, Figure 2c), and partial correlations with temperature, precipitation and VPD vary across a large range from negative to positive
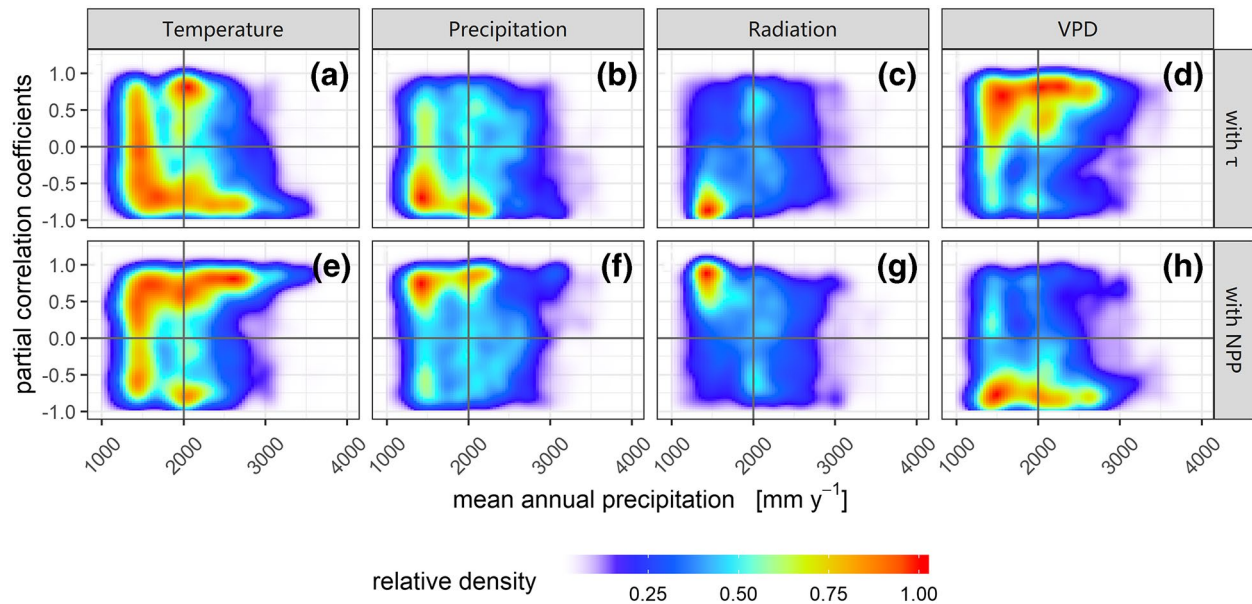
Figure 2. Heat-maps of partial correlation coefficients with turnover time (τ) and NPP along MAP gradient. Four columns of panels are for temperature (a and e), precipitation (b and f), radiation (c and g), and VPD (d and h), respectively, while two rows of panels are for τ (a to d) and NPP (e to h). The vertical line in each panel indicates MAP of 2,000 mm·y^{-1} and horizontal line indicates division of negative or positive correlation. Relative density by stretching the original density into the range of 0 to 1 was used to be comparable across different panels. Only significant correlation coefficients in grid cells in N+T− and N−T+ regions (see Figure 1c) are shown here. MAP, mean annual precipitation; NPP, net primary production; VPD, vapor pressure deficit.

values (i.e., −1.0 to 0.9, −0.9 to 0.5, and −0.2 to 1.0, respectively, see in Figures 2a, 2b, and 2d). In wetter grid cells where MAP >2,000 mm·y^{-1}, the partial correlations with temperature, precipitation and VPD have a more mono-modal distribution (Figures 2a, 2b, and 2d), while correlations with radiation are weak.

Compared to the partial correlations between τ and climate variables (Figures 2a and 2d), a generally reversed pattern is shown for NPP (Figures 2e and 2h) except for some slight differences. For example, there are more positive partial correlation coefficients between NPP and temperature (Figure 2e) than those between τ and temperature towards negative values (compare Figures 2a and 2e), indicating a more unified control of temperature changes on NPP changes than on τ changes. VPD positively correlated to τ in most of grids in our study region (Figure 2d), and it was generally negatively correlated with NPP (Figure 2h). This is expected because MODIS NPP algorithms rely on a VPD sensitivity function in their light use efficiency model (Running & Zhao, 2015). In addition, the partial correlation coefficients between NPP and VPD are more concentrated to negative values (−0.5 to −1.0, Figure 2h) than those between τ and VPD (−0.2 to 1.0, Figure 2d), especially in regions with MAP <2,000 mm·y^{-1}.

Figure 3 shows the partial correlations of τ and NPP with climatic factors in the two major subregions (i.e., N−T+ and N+T−) along the MAP gradient with intervals of 200 mm·y^{-1}. The blue (N−T+) is separated from the green line (N+T−) in Figure 3a, indicating the different impacts of temperature on τ along MAP in these two subregions. In the N+T− grid cells with MAP >2,200 mm·y^{-1}, positive correlations between τ and temperature are found in green line of Figure 3a but the corresponding area is small (Figure 1c, inset). Therefore, in regions with MAP >2,200 mm·y^{-1}, τ is mainly negatively correlated with temperature with prevailing N−T+ as indicated by the blue line in Figure 3a. In the N+T− subregion, the partial correlation between τ and precipitation is persistently negative along the MAP gradient below 2,200 mm·y^{-1} (green line in Figure 3b). In the N−T+ sub region, the coefficients between τ and precipitation are small on average (blue line in Figure 3b). The negative correlations between τ and radiation in regions with MAP <2,000 mm·y^{-1} in Figure 2c are mainly contributed by N+T− grid cells (green line in Figure 3c). The correlations between τ and radiation are generally weak when MAP exceeds 2,200 mm·y^{-1} in the N−T+ subregion (blue line in Figure 3c). In both N−T+ and N+T−, the partial correlation coefficients between τ and VPD are generally positive, except N−T+ grids with MAP around 1,400 mm·y^{-1} and around 3,800 mm·y^{-1}
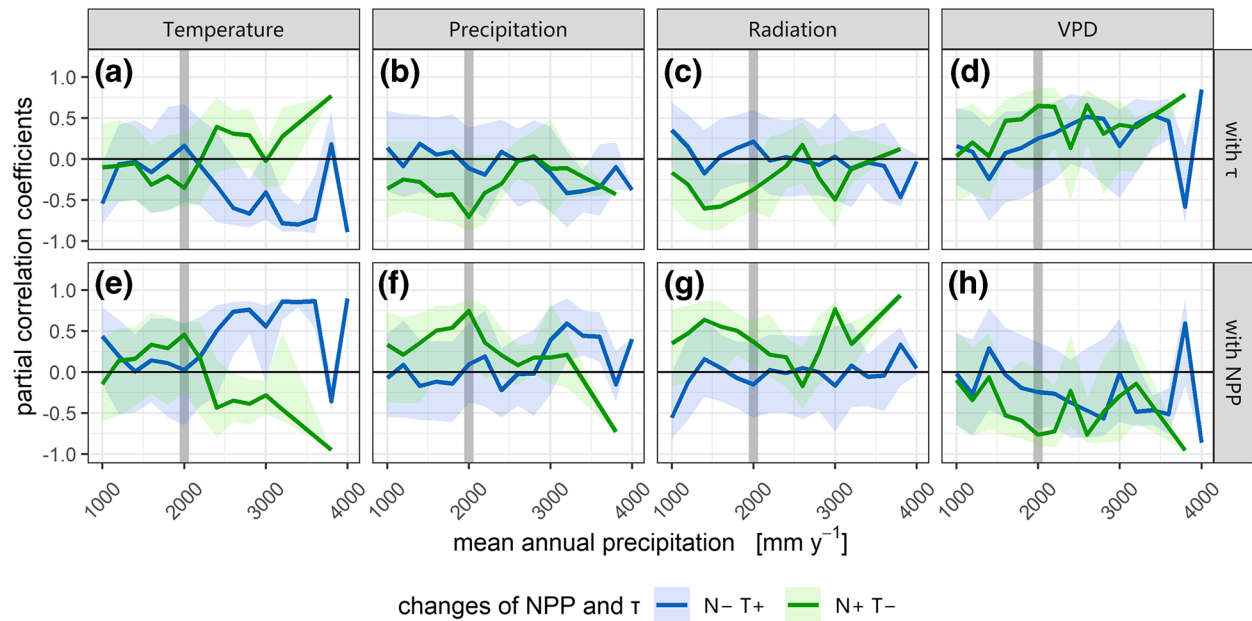
Figure 3. Partial correlations with turnover time (τ) and NPP along MAP gradient. Four columns of panels are for partial correlations with temperature (a and e), precipitation (b and f), radiation (c and g), and VPD (d and h), respectively, while two rows of panels are for τ (a to d) and NPP (e to h). The medians (solid lines) and quartiles (shades) of significant partial correlation coefficients in the two subregions (green for N+T− and blue for N−T+) were shown for each MAP bin of 200 mm·y^{-1}. MAP, mean annual precipitation; NPP, net primary production; VPD, vapor pressure deficit.

where they are negative (Figure 3d), but only 3% and 0.4% of total grid cells are concerned. The partial correlations of NPP with climatic factors in the two major subregions are shown in Figures 3e and 3h, and their patterns are generally reversed from those of τ (Figures 3a and 3d).

3.3. Contributions of Climatic Factors to Turnover Time and NPP Trends

How changes of climatic factors contribute to the trends of τ (or NPP) depends not only on the temporal sensitivities (β_i in Equation 3) but also on the trends of the climatic factors (Figures S13 and S14). That is, if the sensitivity of τ (or NPP) to a climatic factor has the same sign as the trend of this climatic factor, it will contribute to an increment (i.e., positive trend) of τ (or NPP), and vice versa (Figure S14). The temporal trend of τ and NPP can largely be explained by the four climate factors selected with a spatially averaged R^2 of 0.77 for τ (Figure S15) and 0.83 for NPP (Figure S16), while residuals of the multiple linear regression models only contributing small parts (Figures S17 and S18).

Figure 4 summarized the contributions of each factor in the N+T− and N−T+ subregions. In the N+T− subregion (mainly where MAP <2,000 mm·y^{-1}), both precipitation and radiation are associated with decreasing τ trends, with a dominant role of radiation (Figure 4a). This is mainly caused by the negative contributions of radiation and precipitation in central Africa to the τ trends (see Figures S15b and S15c). The dominant contribution of radiation to τ trends in the N+T− grid cells is jointly determined by the negative sensitivity of τ to radiation and the positive radiation trend, which is shown as the hotspot concentrated into the fourth quadrant in Figure S14i. VPD also has considerable negative contributions to τ trends, while the contribution of temperature is minor in the N+T− subregion (Figure 4a). In the N−T+ region (mainly where MAP >2,000 mm·y^{-1}), the contributions of precipitation and radiation to the positive trends of τ are smaller in absolute values than in the N+T− region (Figure 4a), indicating differences in the contributions of climatic factors to τ trends in different subregions. By contrast, temperature and VPD contribute to a large proportion of the increasing τ trends in the N−T+ subregion (Figure 4a), which is driven by their positive contribution in Southeast Asia and western Amazon (Figures S15a and S15d). In these regions, temperature
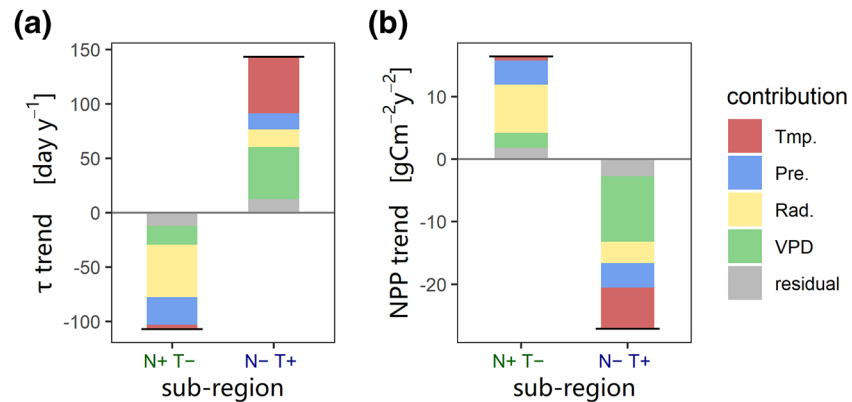
Figure 4. Contribution of temperature, precipitation, radiation, and VPD to the significant trends of turnover time (τ) and NPP in the N+T− and N−T+ subregions. Based on the multiple linear regression in Equation 3, trends of τ (panel a, day·y^{-1}) and NPP (panel b, gC·m^{-2} y^{-2}) were decomposed into contributions of climatic variables ($\beta_i \frac{x_i}{dt}$ in Equation 4) and trends of residuals (in gray). Black lines indicate trends of τ and NPP. NPP, net primary production; VPD, vapor pressure deficit.

mainly has decreasing trends (Figure S13a) and negatively correlates to τ (Figure S11a), while VPD has mainly increasing trends (Figure S13d) and positively correlates to τ (Figure S11d).

Compared to their contributions to τ trends (Figure 4a and Figure S15), climatic factors generally have similar contributions to NPP trends, but with an opposite sign (Figure 4b and Figure S16). Still, there are some differences. For example, VPD has more relative contributions to the NPP trends than the τ trends in the N−T+ region. In turn, temperature contributed relatively less to the NPP trends than to the τ trends. In addition, VPD tends to suppress rather than stimulate NPP, because VPD generally has negative correlations with NPP and increasing trends in the N−T+ region (Figure 4b and Figures S12d, S13d, and S14p).

4. Discussion

4.1. Factors Contributing to Changes of Turnover Time and NPP

We analyzed the temporal correlations between τ and climatic factors in this study. Some previous studies also focused on vegetation carbon turnover time globally or regionally but on the spatial relationships between external factors and τ instead of temporal correlations (Carvalhais et al., 2014; J. Wang et al., 2018; Wu et al., 2018). Our temporal correlation coefficients show high spatial heterogeneity, which may not be reflected in the spatial correlations. For example, the signs of partial correlation coefficients between temperature and τ in the N+T− and N−T+ subregions are different across a MAP threshold of about 2,000 mm·y^{-1} in (Figure 3a), but Wu et al. (2018) showed a generally positive spatial correlation between temperature and τ in tropics. The relatively uniform correlation coefficients and regression coefficients may be caused by the multiyear mean data (2000–2005) they used and by the close association among neighbor grids when calculating spatial correlation and fitting the multiple linear regression (Wu et al., 2018). Therefore, temporal correlations could provide more direct evidence to understand how transient turnover time may change in future climate by excluding the possible biases raised by spatially heterogeneous soil conditions in the spatial correlation.

In regions with MAP <2,000 mm·y^{-1}, both positive and negative partial correlations of temperature with τ or NPP were found (Figures 2a and 2e), which resulted in an unclear contribution of temperature to τ and NPP trends (Figure 4). Tropical forest is not limited by temperature; on the contrary, excessive temperatures may exceed the optima of tropical forest to sequestrate carbon and enhance water-stress in the precipitation-limited regions (Corlett, 2011; Huang et al., 2019; Samaniego et al., 2018). Where precipitation is not limiting (i.e., MAP >2,000 mm·y^{-1} in this study), higher temperature tends to further accelerate turnover processes (decrease of τ) and enhance productivity over the study period (Figures 2a and 2e and the blue

line of Figures 3a and 3e). Precipitation mainly has negative correlation with τ and positive correlation with NPP in regions with MAP <2,000 mm·y^{-1} (Figures 2b and 2f). Increasing precipitation trends in arid regions (such as some regions in Africa) would alleviate the potential water stress and may explain increases in NPP and decreases in τ (Phillips et al., 2009). Although less rainfall (and the potential drought induced) may increase litter fall and mortality rate and accelerate turnover (decrease τ) in regions with MAP <2,000 mm·y^{-1}, the negative correlation between precipitation and τ are dominated by its dependence on NPP (Figures 2b and 2f). Where vegetation is less limited by water (e.g., MAP >2,500 mm·y^{-1} in Figure 2f), more rainfall will not always stimulate NPP, which is partly revealed by the responses of vegetation index to precipitation from Guan et al. (2015). Similarly, Ahlström et al. (2017) also found a threshold of ~2,000 mm·y^{-1} in the Amazon rainforest, below which evapotranspiration, GPP and biomass increase with precipitation but become saturated above.

Although radiation has no direct impact on the turnover processes, τ and radiation are negatively correlated in regions with MAP <2,000 mm·y^{-1} (Figure 2c and central Africa in Figure S11). This may be because τ is linked with NPP (Schlenger et al., 2019; Stephenson & van Mantgem, 2005) from its definition (Equation 1) and more solar radiation absorbed will increase carbon input through NPP. In the regions with MAP <2,000 mm·y^{-1}, NPP is strongly positively correlated with radiation (Figure 2g). In central Africa where MAP <2,000 mm·y^{-1}, increasing radiation (Figure S13c) accompanied by the increasing rainfall (Figure S13b, which alleviated water stress caused by radiation-driven evapotranspiration) largely contributed to increasing NPP trends (Figure S16b). More solar radiation absorbed in the regions with MAP <2,000 mm·y^{-1}, indirectly changed τ because of its disproportionate impacts on NPP and carbon efflux. In regions with MAP >2,000 mm·y^{-1}, more clouds limit radiation available for vegetation and thus radiation may also limit productivity (Huete et al., 2006; Seddon et al., 2016). However, the temporal correlations between radiation and NPP or τ in these regions are generally weak (Figures 2g and 3g). Optical satellite measurements of productivity are generally limited to cloud-free days, so they may be biased over wet tropical forests. Small temporal variations of radiation there (coefficient of variation is 2.3%) during this period may also limits its contribution to NPP or τ trend.

VPD positively correlated to τ in most of grids in our study region (Figures 2d and 3d), and it was generally negatively correlated with NPP (Figures 2h and 3h). This is expected because VPD was used as a predictor variable in the MODIS NPP algorithms (Running & Zhao, 2015). Higher VPD is also associated with droughts (Park Williams et al., 2013), which may suppress NPP (Cleveland et al., 2011; Novick et al., 2016; Zhao & Running, 2010) or change its allocation among different organs (Doughty et al., 2015; Girardin et al., 2016). Trends of τ may be indirectly affected by the impacts of VPD on NPP because of the covariance between NPP and τ (see in Section 4.3).

In this study, drivers for trends of τ and NPP were analyzed after overlaying a fire mask. Many processes could be impacted by the fire regime which is controlled partly by climate (Mitchard, 2018). For example, fire driven by extreme high temperature and low rainfall may promote tree mortality rate, cause large CO_2 emission from biomass, induce forest edge effects and determine succession of species (Brando et al., 2019; Deklerck et al., 2019; Pellegrini et al., 2017; Pugh et al., 2019). We applied a fire mask in our analyses since we only aimed to reveal the direct contribution of climatic factors on τ and NPP without being affected by fire disturbance. Therefore, we note here that the indirect effects (e.g., climate induced fires) on τ are not included in this study. In addition, due to lack of appropriate datasets, disturbances like pest outbreak (Nair, 2001) and windstorm (Magnabosco Marra et al., 2018) are not considered specifically in our study. In addition to temperature, precipitation, radiation, and VPD, other external factors like soil moisture and atmospheric dryness should also influence the trends of τ and NPP (e.g., drought events across Amazon forest in 2005 and 2010) (Doughty et al., 2015; Green et al., 2019; Trugman et al., 2018). However, temperature, precipitation, radiation and VPD represent the major factors controlling the biophysical processes that are directly related to biomass change (Seddon et al., 2016). Soil moisture largely depends on evapotranspiration and precipitation, indicating that soil moisture effects may indirectly be represented by a combination of temperature and precipitation (Dorigo et al., 2017; Humphrey et al., 2017). Although soil moisture may bring in some lag effects of climate conditions, a lack of gridded soil moisture dataset (e.g., a large data gap in the ESA CCI soil moisture dataset (Dorigo et al., 2017)) limits its use for the multiple linear regressions in our study. Similarly, atmospheric aridity is related to temperature and precipitation (Park Williams

et al., 2013), and its impacts on forest TBC can be mostly expressed by the impacts of VPD (Anderegg et al., 2018; Novick et al., 2016; Zhou et al., 2019).

Climate conditions in the tropics are tightly associated to ENSO events, which further control forest dynamics and the carbon cycle (Zhang et al., 2018). We calculated the Kendall rank correlation between Multivariate ENSO Index (MEI (Wolter & Timlin, 2011), https://www.esrl.noaa.gov/psd/enso/mei/) and τ or NPP. Correlations between MEI and τ or NPP (Figure S19) have similar patterns as trends of τ or NPP (Figures 1a and 1b), although with few significant correlation coefficients. The response of NPP to ENSO events is consistent with former studies (Bastos et al., 2013), with increased NPP along the Pacific coast and decreased along the Atlantic coast. The decreased τ during the El Niño years may result from higher mortality induced by droughts (Laurance Susan et al., 2009; Leitold et al., 2018) or lower wood NPP allocation (Rifai et al., 2018). ENSO events change temperature and precipitation differently across different regions in tropics, which further determine water availability for forest production (Bastos et al., 2013; Laurance Susan et al., 2009).

4.2. Robustness of Turnover Time and NPP Trends

We calculated trends and temporal correlations using data from a relatively short period (2001–2012) which may also induce some uncertainties. To assess the significance of trends of τ and NPP statistically, we tested the trends by MK methods and calculate the difference of mean values between the two-half segments of our study period (i.e., the period before 2006 and the period after 2006). The MK test results (Figure S20) and the difference of mean values between the two-half segments of our study period (Figure S21) are generally consistent with the linear trends of τ and NPP (Figures 1a and 1b), verifying our analyses based on MODIS products in the study period.

We also calculated the relative trend and detrended coefficient of IAV to investigate the temporal variation of NPP, τ and biomass. The relative biomass trends range from 0% and 1.1% per year (90% CI, confidence interval, and the median = 0.07%, the same below) across the tropical forest (Figure S22c). The relative trends of NPP and τ range from 0.16% to 2.9% per year (median = 0.09%, Figure S22a) and from 0.22% to 4.1% per year (median = 1.3%, Figure S22b), respectively. Relative trends of NPP are much larger than biomass in most of the grid cells. By contrast, in some grid cells in southeastern Amazon and western Indonesia, relative trends of biomass are higher than that of NPP. The spatial distributions of detrended IAV of NPP, τ and biomass (Figure S23) are generally similar to relative trends (Figure S22) in Southeast Asia and Africa but different in South America. In Southeast Asia, both IAVs and relative trends are high and decrease from west to east (Figures S22 and S23). In central Africa, relative trends of NPP and τ are much higher in the Congo basin than the surrounding area (Figure S22), but spatial gradients for IAVs are less noticeable (Figure S23). In South America, the high relative trends of NPP and τ mainly appear in grid cells near Peru, and southwestern Amazon (Figure S22), while the high IAV values of NPP and τ mainly appear in southeastern Amazon (Figure S23).

In addition, as described in Section 2.5, NPP from the other three datasets were used to calculate forest NPP and τ in tropics and to verify our results based on MODIS NPP, which were shown in the supporting information (Figures S24–S27). Although NPP from BESS and Stocker19 were also based on MODIS FPAR or LAI, they used different algorithms. By contrast, the algorithms to produce GIMMS NPP data are the same as MODIS NPP but with different input data (Section 2.5). Results based on GIMMS NPP and on NPP from BESS and Stocker19 are generally in agreement with MODIS NPP with some slight differences (Figure 1 and Figures S24–S27). For example, there were less significant trends of NPP or τ based on the GIMMS dataset (Figure S24), and temperature had a less negative contribution to trends of τ in N+T− subregion with this dataset (Figure S27b). Although the GIMMS NPP has a similar spatial distribution as BESS and Stocker19 (Figure S1), the time period of GIMMS NPP is 1 year shorter and the resolution (1°) is coarser, which may partly account for the difference. As a whole, results from all four NPP data sources showed a similar spatial distribution of subregions as well as a similar threshold of MAP ≈ 2,000 mm·y^{-1} that delineate the N+T− and N−T+ subregions (Figure 1 and Figure S24).

4.3. Assessment of Uncertainties

We deduced the turnover time by taking transient changes in TBC into account rather than using the ratio between TBC and NPP by assuming a steady state of the carbon pool in previous studies (De Kauwe et al., 2014; Wu et al., 2018). Still, the deduced τ in this study (Equation 1) is not fully decoupled with NPP as reflected by the generally reverse patterns between τ and NPP. NPP contributes 60.1% ± 14.7% to temporal variation of τ in our study region, while TBC contributes 20.7% ± 18.2% (Figure S28). Although impact of TBC on τ trend cannot be neglected (e.g., the same signs of trends for τ and dTBC in a few grid cells shown in Figure S29, the trend of τ is mainly inherited from NPP because the trends of TBC and dTBC are generally weak (Figure S2b) or nonsignificant (Figures S29 and Figure S30e). Although NPP and the deduced τ are not fully decoupled, they have different ecological implications. On the one hand, turnover time in biomass is impacted by carbon input flux (i.e., NPP), allocation of NPP, and carbon output fluxes (i.e., processes like litter fall and mortality, disturbances like fire, drought, insect, etc.). Therefore, NPP is indeed physically connected to τ. On the other hand, it is still disputable in how to represent τ, and most studies used mass/flux as an approximation, which may largely reflect the changes in turnover rate. To better represent τ, differences in turnover processes among various carbon pools (Lu et al., 2018; Sierra et al., 2018) should be considered. To our knowledge, there is no large-scale observation based data to explicitly represent turnover processes of multiple pools and the carbon transit time is only possibly calculated by some process-based models, some specific field experiments or with the help of stable isotopes (Lu et al., 2018).

In this study, uncertainties in τ trends are inherited from uncertainties in biomass and NPP data we used. Uncertainties and the assessments were summarized in Table S3. To validate results based on MODIS NPP, we calculated the results based on BESS, GIMMS and Stocker19 datasets and they generally agree with MODIS NPP (Figures S24–S27). However, it is worth mentioning that these datasets are not fully independent from MODIS NPP (Table S1). These associations mainly include the same algorithms as MOD17A3 products, input data based on MODIS products or the CUE (deduced from MODIS NPP/GPP) used to convert NPP from GPP in BESS and Stocker19.

GIMMS NPP is calculated with the same algorithm as MODIS NPP but based on GIMMS products (i.e., FPAR3g and LAI3g) and different climatic datasets (Smith et al., 2016; Zhu et al., 2013). The algorithms to generate FPAR3g and LAI3g were trained by the MODIS FPAR and LAI, and these algorithms were then applied to AVHRR NDVI to generate GIMMS FPAR3g and LAI3g (Zhu et al., 2013). BESS GPP, which coupled processes such as radiation transfer, photosynthesis and evapotranspiration, used 7 MODIS products (Table S1, including MODIS LAI) and other 11 datasets as inputs (C. Jiang & Ryu, 2016; Ryu et al., 2011). One of input data for GPP from Stocker19 was FPAR3g (Stocker et al., 2019), which may relate to MODIS FPAR as we discussed before. Climate variables, atmospheric CO_2 concentration and soil moisture were also included in the P-model to derive GPP (Stocker et al., 2019; H. Wang et al., 2017).

In this study, CUE from MOD17A3 products was used to calculate NPP from BESS and Stocker19 in each year, which make these products not fully independent from MODIS NPP. Distribution of MODIS CUE trends are similar to MODIS NPP (see Figure S6b and Figure 1b), while the distributions of GPP trends from BESS and Stocker19 (Figures S31a and S31b) are rather different from their NPP trends derived from GPP (which are more similar to MODIS NPP, Figure S8). In order to compare the contributions of MODIS CUE and GPP to the trend of derived NPP, we calculated their relative trends and decomposed the trend of derived NPP into the trend induced by GPP and the trend induced by CUE (see Text S1 and Figures S32–S34 for detail). Relative trends of MODIS CUE are generally twice larger than BESS GPP and Stocker19 GPP and relative trends of CUE overwhelm the relative trends of GPP in most regions (Figure S32). Although the spatial distribution of NPP trends is mainly contributed by MODIS CUE (91% and 73% for NPP derived from BESS and Stocker19 GPP, respectively), contributions of BESS GPP (9%) and Stocker19 GPP (27%) are not negligible (Text S1).

We applied a time-invariant CUE (i.e., mean MODIS CUE during 2001–2012, temporally constant but spatially variant) on BESS and Stocker19 GPP to remove the impact of MODIS CUE on trends of the derived NPP. The trends of NPP and τ based on the time-invariant CUE (Figure S35) are generally insignificant and different from the results based on time-variant MODIS CUE (Figure S24). Only in the northeast region of South America, the "N+T−" trends are consistent in both MODIS NPP (Figure S24) and the alternative NPP

derived by the time-invariant CUE (Figure S35). In other regions, using time-invariant CUE trends largely changed the patterns of NPP and τ trends. Therefore, the trends of NPP derived from BESS and Stocker19 GPP and MODIS CUE (Figure S24) are largely driven by the temporal trends in MODIS CUE. The robustness of MODIS CUE thus determines the robustness of trends in the derived NPP. That is if the MODIS CUE is reliable, the spatial patterns from BESS and Stocker19 would be similar to the MODIS NPP, which could verify the results derived from MODIS NPP data.

In order to assess the MODIS CUE, we collected field observation CUE data from Collalti et al. (2019) and Malhi et al. (2015). Within our study region, 21 plot observations for tropical forest CUE were selected (Figure S36). After merging field plots in the same 0.25° grid cells, observed CUE values in ten 0.25° grid cells were compared with MODIS CUE used in our study (Figure S37 and Table S4). In general, MODIS CUE can reproduce 7 out of 10 observations with error bars crossing the 1:1 line (Figure S37), implying consistency between the MODIS CUE and the observed CUE. The two mismatched sites are located in Xishuangbanna in China (mean observed CUE = 0.38 and mean MODIS CUE = 0.52, #9 in Figures S36 and S37 and Table S4) and in Tambopata in Peru (mean observed CUE = 0.42 and mean MODIS CUE = 0.60, #3 in Figures S36 and S37 and Table S4). Both sites lie on the regions with a high MODIS CUE (Figure S36 and Table S4), indicating that MODIS may overestimate the CUE. The observed CUE is generally smaller than 0.5. By contrast, MODIS CUE is greater than 0.5 in some regions like northern Indo-China Peninsula, northeastern Amazon and along the Andes (Figure S36). MODIS CUE in these regions may be overestimated because MODIS CUE in the tropics largely relies on the meteorological inputs which contains high uncertainties in the high elevations (Cleveland et al., 2015). Fortunately, in these regions with possible CUE overestimation, the trends of derived NPP from MODIS CUE and BESS GPP or Stocker19 GPP are mainly contributed by GPP instead of CUE (Figures S33 and S34). Therefore, the uncertainty of CUE in these regions may have little impact on the NPP trends. Actually, we compared the field observed NPP trends with MODIS NPP trends (Text S2, Figures S38–S40), and the trends are generally consistent on a regional scale (Figures S39 and S40).

We should however remain cautious about MODIS CUE trends because of the underlying assumptions regarding autotrophic respiration. MODIS assumes a biome-type based constant fraction of GPP as growth respiration fraction and a high sensitivity of maintenance respiration to temperature (see details in the User's Guide of MOD17A2/A3 from (Running & Zhao, 2015). In contrast, plant respiration may be slightly changed by temperature variation because of thermal acclimation (Gifford, 2003; O'Leary et al., 2019; Reich et al., 2016). The globally high Q10 value in MODIS algorithms has been challenged by Medlyn (2011). Zhao and Running (2011) therefore tested different Q10 values and showed that the mean annual global NPP changed little with different Q10 values. They further checked the NPP trends after reducing Q10. The NPP trend during 2000–2009 decreased from −0.0548 to −0.0061 PgC·y^{-2}, but the direction of global NPP trend didn't change from negative to positive and the interannual variability of NPP changed little. In addition, algorithms of MODIS CUE don't consider a lagged effect of plant response to temperature (Atkin & Tjoelker, 2003; Wen et al., 2018) and effect of elevated CO_2 fertilization effect (Running et al., 2004; Running & Zhao, 2015), which may also contribute to CUE trends. However, due to lack of time series of observed CUE, it is not possible to independently verify the MODIS CUE trends. Although the mean values of CUE across different field studies are very close (e.g., 0.47 based on literatures in Waring et al. (1998) and 0.46 based on literatures in Collalti and Prentice (2019)), considerable variations of CUE may be caused by forest type, stand age, climatic and soil conditions, disturbance and management (Collalti & Prentice, 2019). Therefore, the CUE trends in the tropical forest still need to be confirmed by future research with long-term observations of CUE.

Trends from field data were used to test the results based on satellite observation in our study as described in Section 2.5 and Text S2. On a regional scale, NPP from field observations are generally lower than MODIS NPP (Figure S39) and there are differences in the magnitude of trends, especially in the N−T+ subregion of Amazon where the field data shows a very weak trend compared to the strong trend of MODIS NPP (Figure S39c). But the overall trends from field observations are in the same direction as the MODIS NPP trends on a regional scale (i.e., N+ or N−, Figure S39). τ calculated from the field observations are generally higher than τ based on satellite data. Similarly, the field observation based τ trends agree with the satellite based τ trends on a regional scale (Figures S40a, S40c, and S40d) except in the N+T− subregion in tropical Africa

(Figure S40b), probably due to the large variations across different sites. It should be noted that the increasing trend of τ in the N−T+ subregion in tropical Africa is mainly driven by the high τ value (1,292 years) in 2012 (Figure S40a) since the field data are very limited, which is consistent with the few area of N−T+ subregion in tropical Africa (Figure 1c). The comparison of NPP and τ trends (Figures S39 and S40) is based on a regional scale and thus partly avoids the impacts of extreme values and large variations at one single site and the strong heterogeneity in the whole 0.25° grids.

In this study, when converting ABC to TBC, the constant TBC/ABC ratio (1.26 for tropical forest) may not reflect the heterogeneity across tropics and may also enlarge the uncertainty of separation between forest and non-forest biomass. In order to evaluate the uncertainty induced by the constant TBC/ABC ratio (1.26 used in this study), we used the range of this ratio (1.19–1.49) reported in previous studies for tropics (see Table S4 in Liu et al. (2015)). We assigned the TBC/ABC in each tropical grid cell randomly by assuming an even distribution from 1.19 to 1.49 (Figure S41) and recalculated τ and the corresponding trends. Although the random TBC/ABC ratios changed magnitudes of τ and τ trends, the direction of τ trends was little changed (Figure S42), because the temporal variations of τ are mainly contributed by NPP instead of biomass. Therefore, the uncertainty caused by the TBC/ABC ratio has a very small impact on our major results.

The annual biomass data we used is deduced from X-band VOD retrievals (Liu et al., 2015), which may saturate when biomass is high in the tropical forest (Rodríguez-Fernández et al., 2018; Chaparro et al., 2019). From Figure S43a, biomass based on X-band VOD retrievals in tropical forest generally saturate at 18 kgC·m^{-2}. Biomass in regions with actual biomass above 18 kgC·m^{-2} may be insensitive to climate variations and contribute little to τ trend calculation (i.e., dTBC $\approx$ 0 in Equation 1), which result in the strong covariance between τ and NPP as we discussed before. In addition, X-band VOD may be more sensitive to canopy water content than to stem water content because of its shorter wavelength (Rodríguez-Fernández et al., 2018). The significant positive correlation between biomass and mean annual MODIS C6 FPAR (resampled into 0.25°, Figure S43b) partly supports the connection between biomass and leaf density. Still, biomass based on X-band VOD may reflect some signals of woody parts, because biomass continues to increase from 7 to 15 kgC·m^{-2} when FPAR becomes relatively flat (Figure S43b).

To assess biomass data from Liu et al. (2015), we first used satellite-based biomass data from Baccini et al. (2017). Because the annual biomass data from Baccini et al. (2017) are not publicly available, we only used the released biomass gain and loss for the whole period of 2003–2014 to assess biomass data from Liu et al. (2015). We resampled the aboveground biomass gain and loss (500 × 500 m) from Baccini et al. (2017) into 0.25° grid cells and merged them into the net changes. Net changes of forest aboveground biomass during 2001–2012 from Liu et al. (2015) were then compared against the net changes during 2003–2014 from Baccini et al. (2017) in Figure S44 and Table S5. The net changes from Liu et al. (2015) are generally lower than the net changes from Baccini et al. (2017) in most tropical forest regions, but the directions of net changes are overall consistent (Figure S44 and Table S5). In Africa, biomass from Baccini et al. (2017) shows net loss in the Congo basin and net gains in the surrounding regions (Figure S44a), but biomass data from Liu et al. (2015) only shows net gain in the surrounding regions (Figure S44b). In South America, net biomass loss appears in most grid cells from Baccini et al. (2017) (Figure S44a), but the signal is only strong in the Southeast Amazon from Liu et al. (2015) (Figure S44b). The weaker biomass loss from Liu et al. (2015) in South America and tropical Africa (Figure S44) can be also reflected by the lower continental net changes in Table S5. In tropical Asia, biomass from Liu et al. (2015) shows stronger loss in Malaysia and West Indonesia but weaker gain in India and the northern parts of Indo-China Peninsula compared with biomass from Baccini et al. (2017) (Figure S44), which results in a larger carbon loss from Liu et al. (2015) in Table S5.

Aboveground biomass and the fitted linear trends from Liu et al. (2015) were also compared with 136 field observations in Amazon from Brienen et al. (2015). In Figure S45, the biomass magnitude and trend from Liu et al. (2015) are both lower than the field observations, but the overall trend from Liu et al. (2015) is in the same direction as the trend from field observations. Although the dataset from Liu et al. (2015) may underestimate biomass and be insensitive to biomass change due to the saturation of X-band VOD in the tropical forest, the directions of the trends are generally consistent with field based estimates both indicating a slight increase in tropical biomass over the period of analysis.

In addition, the temporal resolution (annually) from Liu et al. (2015) may hide the effects of seasonal climate conditions (e.g., cooling trends of seasonal temperature during September to November as pointed out by (Cohen et al., 2012)). Also, the spatial resolution (0.25°) may be difficult to validate by field data and to separate forest and non-forest grid cells directly (i.e., the methods for separation in Section 2.2 may also bring uncertainties). However, biomass data with finer resolution (Baccini et al., 2017; Bouvet et al., 2018) as far as we can access are not temporally resolved so that can't be used to analyze the temporal changes as we do in this study.

5. Conclusion

Although many factors may contribute to changes of turnover time and NPP, the combination of temperature, precipitation, radiation and VPD represents most part of climatic impacts. Transient turnover time and its temporal association with climatic variables reveal the impacts of climate change on turnover time more directly than spatial correlation which may be biased by heterogeneity of soil condition. However, limited by the availability of long-term and large-scale observation based data, the long-term capability of carbon sequestration in tropical forest biomass cannot be fully assessed at this stage. In addition, the spatial patterns of τ and NPP trends seem to depend largely on the CUE trends from MODIS because NPP trends are very sensitive to the CUE trend. Although the mean MODIS CUE generally agree with the mean CUE from field observations, uncertainties in CUE trends are not verifiable based on current knowledge and available data, and we should remain cautious when interpreting the results. It therefore calls for more observations of CUE trends in the future. In addition, long-term biomass data with finer resolution and better quality would improve the accuracy of the deduced turnover time and offer more insights for understanding tropical forest dynamics under future climate change.

Data Availability Statement

The original MODIS C6 FPAR data (MODIS FPAR product (MOD15A2H) Collection 6) is available through Chen et al. (2017) and can be downloaded from U.S. Geological Survey (https://lpdaac.usgs.gov/products/mod15a2hv006/). MODIS NPP dataset (MOD17A3) is available from U.S. Geological Survey (https://lp-daac.usgs.gov/products/mod17a3hv006/). The temperature and precipitation datasets are the public data from Climate Research Unit (CRU TS version 4.02, https://crudata.uea.ac.uk/cru/data/hrg/cru_ts_4.02/cruts.1811131722.v4.02/). The fire dataset is available from the fire projects of European Space Agency Climate Change Initiative (CCI) (Fire_CCI, http://www.esa-fire-cci.org/). The 2-m air temperature and specific humidity datasets are available from Climatic Research Unit and Japanese Meteorological Agency reanalysis (CRU JRA V1.1, University of East Anglia Climatic Research Unit; Harris (2019)). The Stocker19 GPP data is available through Stocker et al. (2019) (https://zenodo.org/record/1423484). The BESS GPP data is available through C. Jiang and Ryu (2016) and can be downloaded from http://environment.snu.ac.kr/bess_flux/. The radiation data is available through Ryu et al. (2018) and can be downloaded from http://environment.snu.ac.kr/bess_rad/.

References

Ahlström, A., Canadell, J. G., Schurgers, G., Wu, M., Berry, J. A., Guan, K., et al. (2017). Hydrologic resilience and Amazon productivity. *Nature Communications*, *8*(1), 387. https://doi.org/10.1038/s41467-017-00306-z

Anderegg, W. R. L., Konings, A. G., Trugman, A. T., Yu, K., Bowling, D. R., Gabbitas, R., et al. (2018). Hydraulic diversity of forests regulates ecosystem resilience during drought. *Nature*, *561*(7724), 538–541. https://doi.org/10.1038/s41586-018-0539-7

Atkin, O. K., & Tjoelker, M. G. (2003). Thermal acclimation and the dynamic response of plant respiration to temperature. *Trends in Plant Science*, *8*(7), 343–351. https://doi.org/10.1016/S1360-1385(03)00136-5

Baccini, A., Walker, W., Carvalho, L., Farina, M., Sulla-Menashe, D., & Houghton, R. A. (2017). Tropical forests are a net carbon source based on aboveground measurements of gain and loss. *Science*, *358*(6360), 230–234. https://doi.org/10.1126/science.aam5962

Bastos, A., Running, S. W., Gouveia, C., & Trigo, R. M. (2013). The global NPP dependence on ENSO: La Niña and the extraordinary year of 2011. *Journal of Geophysical Research: Biogeosciences*, *118*(3), 1247–1255. https://doi.org/10.1002/jgrg.20100

Bonan, G. B. (2008). Forests and climate change: Forcings, feedbacks, and the climate benefits of forests. *Science*, *320*(5882), 1444–1449. https://doi.org/10.1126/science.1155121

Bouvet, A., Mermoz, S., Le Toan, T., Villard, L., Mathieu, R., Naidoo, L., et al. (2018). An above-ground biomass map of African savannahs and woodlands at 25 m resolution derived from ALOS PALSAR. *Remote Sensing of Environment*, *206*, 156–173. https://doi.org/10.1016/j.rse.2017.12.030

Brando, P. M., Silvério, D., Maracahipes-Santos, L., Oliveira-Santos, C., Levick, S. R., Coe, M. T., et al. (2019). Prolonged tropical forest degradation due to compounding disturbances: Implications for CO_2 and H_2O fluxes. *Global Change Biology*, *25*(9), 2855–2868. https://doi.org/10.1111/gcb.14659

Brienen, R. J. W., Phillips, O. L., Feldpausch, T. R., Gloor, E., Baker, T. R., Lloyd, J., et al. (2015). Long-term decline of the Amazon carbon sink. *Nature*, *519*(7543), 344–348. https://doi.org/10.1038/nature14283

Carvalhais, N., Forkel, M., Khomik, M., Bellarby, J., Jung, M., Migliavacca, M., et al. (2014). Global covariation of carbon turnover times with climate in terrestrial ecosystems. *Nature*, *514*(7521), 213–217. https://doi.org/10.1038/nature13731

Chaparro, D., Duveiller, G., Piles, M., Cescatti, A., Vall-llossera, M., Camps, A., et al. (2019). Sensitivity of L-band vegetation optical depth to carbon stocks in tropical forests: A comparison to higher frequencies and optical indices. *Remote Sensing of Environment*, *232*, 111303. https://doi.org/10.1016/j.rse.2019.111303

Chen, C., Knyazikhin, Y., Park, T., Yan, K., Lyapustin, A., Wang, Y., et al. (2017). Prototyping of LAI and FPAR retrievals from MODIS Multi-Angle Implementation of Atmospheric Correction (MAIAC) data. *Remote Sensing*, *9*(370), 1–17. https://doi.org/10.3390/rs9040370

Chuvieco, E., Sandow, C., Guenther, K. P., Gonzalez-Alonso, F., Pereira, J. M., Perez, O., et al. (2012). *Global burned area mapping from European satellites: The ESA FIRE_CCI project*. Paper presented at the International Archives of the Photogrammetry Remote Sensing and Spatial Information Sciences. Retrieved from http://gateway.isiknowledge.com/gateway/Gateway.cgi?GWVersion=2&SrcAuth=AegeanSoftware&SrcApp=NoteExpress&DestLinkType=FullRecord&DestApp=WOS&KeyUT=000358207600003

Cleveland, C. C., Taylor, P., Chadwick, K. D., Dahlin, K., & Townsend, A. R. (2015). A comparison of plot-based, satellite and Earth system model estimates of tropical forest net primary production: NPP IN TROPICAL FORESTS. *Global Biogeochemical Cycles*, *29*(5), 626–644.

Cleveland, C. C., Townsend, A. R., Taylor, P., Alvarez-Clare, S., Bustamante, M. M. C., Chuyong, G., et al. (2011). Relationships among net primary productivity, nutrients and climate in tropical rain forest: A pan-tropical analysis. *Ecology Letters*, *14*(12), 1313–1317. https://doi.org/10.1111/j.1461-0248.2011.01711.x

Cohen, J. L., Furtado, J. C., Barlow, M., Alexeev, V. A., & Cherry, J. E. (2012). Asymmetric seasonal temperature trends. *Geophysical Research Letters*, *39*(4), L04705–L04705. https://doi.org/10.1029/2011GL050582

Collalti, A., & Prentice, I. C. (2019). Is NPP proportional to GPP? Waring's hypothesis 20 years on. *Tree Physiology*, *39*(8), 1473–1483. https://doi.org/10.1093/treephys/tpz034

Corlett, R. T. (2011). Impacts of warming on tropical lowland rainforests. *Trends in Ecology & Evolution*, *26*(11), 606–613. https://doi.org/10.1016/j.tree.2011.06.015

Cox, P. M., Pearson, D., Booth, B. B., Friedlingstein, P., Huntingford, C., Jones, C. D., et al. (2013). Sensitivity of tropical carbon to climate change constrained by carbon dioxide variability. *Nature*, *494*(7437), 341–344. https://doi.org/10.1038/nature11882

De Kauwe, M. G., Medlyn, B. E., Zaehle, S., Walker, A. P., Dietze, M. C., Wang, Y., et al. (2014). Where does the carbon go? A model-data intercomparison of vegetation carbon allocation and turnover processes at two temperate forest free-air CO_2 enrichment sites. *New Phytologist*, *203*(3), 883–899. https://doi.org/10.1111/nph.12847

Deklerck, V., De Mil, T., Ilondea, B. A., Nsenga, L., De Caluwé, C., Van den Bulcke, J., et al. (2019). Rate of forest recovery after fire exclusion on anthropogenic savannas in the Democratic Republic of Congo. *Biological Conservation*, *233*, 118–130. https://doi.org/10.1016/j.biocon.2019.02.027

Dorigo, W., Wagner, W., Albergel, C., Albrecht, F., Balsamo, G., Brocca, L., et al. (2017). ESA CCI Soil Moisture for improved Earth system understanding: State-of-the art and future directions. *Remote Sensing of Environment*, *203*, 185–215. https://doi.org/10.1016/j.rse.2017.07.001

Doughty, C. E., Metcalfe, D. B., Girardin, C. A. J., Amézquita, F. F., Cabrera, D. G., Huasco, W. H., et al. (2015). Drought impact on forest carbon dynamics and fluxes in Amazonia. *Nature*, *519*(7541), 78–82. https://doi.org/10.1038/nature14213

Erb, K., Fetzel, T., Plutzar, C., Kastner, T., Lauk, C., Mayer, A., et al. (2016). Biomass turnover time in terrestrial ecosystems halved by land use. *Nature Geoscience*, *9*(9), 674–678. https://doi.org/10.1038/ngeo2782

Friedl, M. A., Sulla-Menashe, D., Tan, B., Schneider, A., Ramankutty, N., Sibley, A., et al. (2010). MODIS Collection 5 global land cover: Algorithm refinements and characterization of new datasets. *Remote Sensing of Environment*, *114*(1), 168–182. https://doi.org/10.1016/j.rse.2009.08.016

Gifford, R. M. (2003). Plant respiration in productivity models: Conceptualisation, representation and issues for global terrestrial carbon-cycle research. *Functional Plant Biology*, *30*(2), 171. https://doi.org/10.1071/FP02083

Girardin, C. A. J., Malhi, Y., Doughty, C. E., Metcalfe, D. B., Meir, P., Del Aguila-Pasquel, J., et al. (2016). Seasonal trends of Amazonian rainforest phenology, net primary productivity, and carbon allocation. *Global Biogeochemical Cycles*, *30*(5), 700–715. https://doi.org/10.1002/2015GB005270

Graham, E. A., Mulkey, S. S., Kitajima, K., Phillips, N. G., & Wright, S. J. (2003). Cloud cover limits net CO_2 uptake and growth of a rainforest tree during tropical rainy seasons. *Proceedings of the National Academy of Sciences of the United States of America*, *100*(2), 572–576. https://doi.org/10.1073/pnas.0133045100

Green, J. K., Seneviratne, S. I., Berg, A. M., Findell, K. L., Hagemann, S., Lawrence, D. M., et al. (2019). Large influence of soil moisture on long-term terrestrial carbon uptake. *Nature*, *565*(7740), 476–479. https://doi.org/10.1038/s41586-018-0848-x

Guan, K., Pan, M., Li, H., Wolf, A., Wu, J., Medvigy, D., et al. (2015). Photosynthetic seasonality of global tropical forests constrained by hydroclimate. *Nature Geoscience*, *8*(4), 284–289. https://doi.org/10.1038/ngeo2382

Harris, I. C. (2019). *CRU JRA v1.1: A forcings dataset of gridded land surface blend of Climatic Research Unit (CRU) and Japanese reanalysis (JRA) data; Jan.1901 - Dec.2017*. Centre for Environmental Data Analysis. Retrived from http://catalogue.ceda.ac.uk/uuid/863a47a6d8414b6982e1396c69a9efe8

Huang, M., Piao, S., Ciais, P., Peñuelas, J., Wang, X., Keenan, T. F., et al. (2019). Air temperature optima of vegetation productivity across global biomes. *Nature Ecology & Evolution*, *3*(5), 772–779. https://doi.org/10.1038/s41559-019-0838-x

Hubau, W., Lewis, S. L., Phillips, O. L., Affum-Baffoe, K., Beeckman, H., Cuní-Sanchez, A., et al. (2020). Asynchronous carbon sink saturation in African and Amazonian tropical forests. *Nature*, *579*(7797), 80–87. https://doi.org/10.1038/s41586-020-2035-0

Huete, A. R., Didan, K., Shimabukuro, Y. E., Ratana, P., Saleska, S. R., Hutyra, L. R., et al. (2006). Amazon rainforests green-up with sunlight in dry season. *Geophysical Research Letters*, *33*(6), L06405–L06405. https://doi.org/10.1029/2005GL025583

Humphrey, V., Gudmundsson, L., & Seneviratne, S. I. (2017). A global reconstruction of climate-driven subdecadal water storage variability. *Geophysical Research Letters*, *44*(5), 2300–2309. https://doi.org/10.1002/2017GL072564

Jiang, C., & Ryu, Y. (2016). Multi-scale evaluation of global gross primary productivity and evapotranspiration products derived from Breathing Earth System Simulator (BESS). *Remote Sensing of Environment*, *186*, 528–547. https://doi.org/10.1016/j.rse.2016.08.030

Jiang, L., Shi, Z., Xia, J., Liang, J., Lu, X., Wang, Y., et al. (2017). Transient traceability analysis of land carbon storage dynamics: Procedures and its application to two forest ecosystems. *Journal of Advances in Modeling Earth Systems*, *9*(8), 2822–2835. https://doi.org/10.1002/2017MS001004

Keenan, R. J., Reams, G. A., Achard, F., de Freitas, J. V., Grainger, A., & Lindquist, E. (2015). Dynamics of global forest area: Results from the FAO Global Forest Resources Assessment 2015. *Forest Ecology and Management*, *352*, 9–20. https://doi.org/10.1016/j.foreco.2015.06.014

Knauer, J., El-Madany, T. S., Zaehle, S., & Migliavacca, M. (2018). Bigleaf—An R package for the calculation of physical and physiological ecosystem properties from eddy covariance data. *PloS One*, *13*(8), e201114. https://doi.org/10.1371/journal.pone.0201114

Koven, C. D., Chambers, J. Q., Georgiou, K., Knox, R., Negron-Juarez, R., Riley, W. J., et al. (2015). Controls on terrestrial carbon feedbacks by productivity versus turnover in the CMIP5 Earth System Models. *Biogeosciences*, *12*(17), 5211–5228. https://doi.org/10.5194/bg-12-5211-2015

Lauenroth, W. K., & Adler, P. B. (2008). Demography of perennial grassland plants: Survival, life expectancy and life span. *Journal of Ecology*, *96*(5), 1023–1032. https://doi.org/10.1111/j.1365-2745.2008.01415.x

Laurance Susan, G. W., Laurance, W. F., Nascimento, H. E. M., Andrade, A., Fearnside, P. M., Rebello Expedito, R. G., et al. (2009). Long-term variation in Amazon forest dynamics. *Journal of Vegetation Science*, *20*(2), 323–333. https://doi.org/10.1111/j.1654-1103.2009.01044.x

Leitold, V., Morton, D. C., Longo, M., Dos Santos, M. N., Keller, M., & Scaranello, M. (2018). El Niño drought increased canopy turnover in Amazon forests. *New Phytologist*, *219*(3), 959–971. https://doi.org/10.1111/nph.15110

Liu, Y. Y., de Jeu, R. A. M., McCabe, M. F., Evans, J. P., & van Dijk, A. I. J. M. (2011). Global long-term passive microwave satellite-based retrievals of vegetation optical depth. *Geophysical Research Letters*, *38*(18), L18402–L18402. https://doi.org/10.1029/2011GL048684

Liu, Y. Y., van Dijk, A. I. J. M., de Jeu, R. A. M., Canadell, J. G., McCabe, M. F., Evans, J. P., et al. (2015). Recent reversal of loss of global terrestrial biomass. *Nature Climate Change*, *5*(5), 470–474. https://doi.org/10.1038/nclimate2581

Lopez-Gonzalez, G., Lewis, S. L., Burkitt, M., & Phillips, O. L. (2011). ForestPlots.net: A web application and research tool to manage and analyse tropical forest plot data. *Journal of Vegetation Science*, *22*(4), 610–613. https://doi.org/10.1111/j.1654-1103.2011.01312.x

Luo, Y., Shi, Z., Lu, X., Xia, J., Liang, J., Jiang, J., et al. (2017). Transient dynamics of terrestrial carbon storage: Mathematical foundation and its applications. *Biogeosciences*, *14*(1), 145–161. https://doi.org/10.5194/bg-14-145-2017

Lu, X., Wang, Y., Luo, Y., & Jiang, L. (2018). Ecosystem carbon transit versus turnover times in response to climate warming and rising atmospheric CO_2 concentration. *Biogeosciences*, *15*(21), 6559–6572. https://doi.org/10.5194/bg-15-6559-2018

Magnabosco Marra, D., Trumbore, S. E., Higuchi, N., Ribeiro, G. H. P. M., Negrón-Juárez, R. I., Holzwarth, F., et al. (2018). Windthrows control biomass patterns and functional composition of Amazon forests. *Global Change Biology*, *24*(12), 5867–5881. https://doi.org/10.1111/gcb.14457

Malhi, Y., Doughty, C. E., Goldsmith, G. R., Metcalfe, D. B., Girardin, C. A., Marthews, T. R., et al. (2015). The linkages between photosynthesis, productivity, growth and biomass in lowland Amazonian forests. *Global Change Biology*, *21*(6), 2283–2295. https://doi.org/10.1111/gcb.12859

Medlyn, B. E. (2011). Comment on "Drought-Induced Reduction in Global Terrestrial Net Primary Production from 2000 Through 2009". *Science*, *333*(6046), 1093.

Mitchard, E. T. A. (2018). The tropical forest carbon cycle and climate change. *Nature*, *559*(7715), 527–534. https://doi.org/10.1038/s41586-018-0300-2

Nair, K. S. S. (2001). *Pest outbreaks in tropical forest plantations: Is there a greater risk for exotic tree species?* Indonesia: Center for International Forestry Research.

Nemani, R. R. (2003). Climate-driven increases in global terrestrial net primary production from 1982 to 1999. *Science*, *300*(5625), 1560–1563. https://doi.org/10.1126/science.1082750

Novick, K. A., Ficklin, D. L., Stoy, P. C., Williams, C. A., Bohrer, G., Oishi, A. C., et al. (2016). The increasing importance of atmospheric demand for ecosystem water and carbon fluxes. *Nature Climate Change*, *6*(11), 1023–1027. https://doi.org/10.1038/nclimate3114

O'Leary, B. M., Asao, S., Millar, A. H., & Atkin, O. K. (2019). Core principles which explain variation in respiration across biological scales. *New Phytol*, *222*(2), 670–686. https://doi.org/10.1111/nph.15576

Pan, Y., Birdsey, R. A., Fang, J., Houghton, R., Kauppi, P. E., Kurz, W. A., et al. (2011). A large and persistent carbon sink in the world's forests. *Science*, *333*(6045), 988–993. https://doi.org/10.1126/science.1201609

Park Williams, A., Allen, C. D., Macalady, A. K., Griffin, D., Woodhouse, C. A., Meko, D. M., et al. (2013). Temperature as a potent driver of regional forest drought stress and tree mortality. *Nature Climate Change*, *3*(3), 292–297. https://doi.org/10.1038/nclimate1693

Pellegrini, A. F. A., Ahlström, A., Hobbie, S. E., Reich, P. B., Nieradzik, L. P., Staver, A. C., et al. (2017). Fire frequency drives decadal changes in soil carbon and nitrogen and ecosystem productivity. *Nature*, *553*(7687), 194–198. https://doi.org/10.1038/nature24668

Phillips, O. L., Aragao, L. E. O. C., Lewis, S. L., Fisher, J. B., Lloyd, J., Lopez-Gonzalez, G., et al. (2009). Drought sensitivity of the Amazon rainforest. *Science*, *323*(5919), 1344–1347. https://doi.org/10.1126/science.1164033

Pugh, T. A. M., Arneth, A., Kautz, M., Poulter, B., & Smith, B. (2019). Important role of forest disturbances in the global biomass turnover and carbon sinks. *Nature Geoscience*, *12*(9), 730–735. https://doi.org/10.1038/s41561-019-0427-2

Raich, J. W., Russell, A. E., Kitayama, K., Parton, W. J., & Vitousek, P. M. (2006). Temperature influences carbon accumulation in moist tropical forests. *Ecology*, *87*(1), 76–87. https://doi.org/10.1890/05-0023

Reich, P. B., Sendall, K. M., Stefanski, A., Wei, X., Rich, R. L., & Montgomery, R. A. (2016). Boreal and temperate trees show strong acclimation of respiration to warming. *Nature*, *531*(7596), 633–636. https://doi.org/10.1038/nature17142

Rifai, S. W., Girardin, C. A. J., Berenguer, E., Del Aguila-Pasquel, J., Dahlsjo, C. A. L., Doughty, C. E., et al. (2018). ENSO Drives interannual variation of forest woody growth across the tropics. *Philosophical Transactions of the Royal Society B: Biological Sciences*, *373*(1760), 1–13. https://doi.org/10.1098/rstb.2017.0410

Rodríguez-Fernández, N. J., Mialon, A., Mermoz, S., Bouvet, A., Richaume, P., Al Bitar, A., et al. (2018). An evaluation of SMOS L-band vegetation optical depth (L-VOD) data sets: High sensitivity of L-VOD to above-ground biomass in Africa. *Biogeosciences*, *15*(14), 4627–4645. https://doi.org/10.5194/bg-15-4627-2018

Running, S. W., Nemani, R. R., Heinsch, F. A., Zhao, M., Reeves, M., & Hashimoto, H. (2004). A continuous satellite-derived measure of global terrestrial primary production. *BioScience*, *54*(6), 547–560. https://doi.org/10.1641/0006-568(2004)054[0547:ACSMOG]2.0.CO;2

Running, S. W., & Zhao, M. (2015). Daily GPP and Annual NPP (MOD17A2/A3) Products NASA Earth Observing System MODIS Land Algorithm. *MOD17 User's Guide* (Version 3.0).

Ryu, Y., Baldocchi, D. D., Kobayashi, H., van Ingen, C., Li, J., Black, T. A., et al. (2011). Integration of MODIS land and atmosphere products with a coupled-process model to estimate gross primary productivity and evapotranspiration from 1 km to global scales. *Global Biogeochemical Cycles*, *25*(4), GB4017–GB4017. https://doi.org/10.1029/2011GB004053

Ryu, Y., Jiang, C., Kobayashi, H., & Detto, M. (2018). MODIS-derived global land products of shortwave radiation and diffuse and total photosynthetically active radiation at 5 km resolution from 2000. *Remote Sensing of Environment*, *204*, 812–825. https://doi.org/10.1016/j.rse.2017.09.021

Saatchi, S. S., Harris, N. L., Brown, S., Lefsky, M., Mitchard, E. T. A., Salas, W., et al. (2011). Benchmark map of forest carbon stocks in tropical regions across three continents. *Proceedings of the National Academy of Sciences*, *108*(24), 9899–9904. https://doi.org/10.1073/pnas.1019576108

Samaniego, L., Thober, S., Kumar, R., Wanders, N., Rakovec, O., Pan, M., et al. (2018). Anthropogenic warming exacerbates European soil moisture droughts. *Nature Climate Change*, *8*(5), 421–426. https://doi.org/10.1038/s41558-018-0138-5

Schlenger, A. J., Libralato, S., & Ballance, L. T. (2019). Temporal variability of primary production explains marine ecosystem structure and function. *Ecosystems*, *22*(2), 331–345. https://doi.org/10.1007/s10021-018-0272-y

Seddon, A. W. R., Macias-Fauria, M., Long, P. R., Benz, D., & Willis, K. J. (2016). Sensitivity of global terrestrial ecosystems to climate variability. *Nature*, *531*(7593), 229–232. https://doi.org/10.1038/nature16986

Sierra, C. A., Ceballos-Núñez, V., Metzler, H., & Müller, M. (2018). Representing and understanding the carbon cycle using the theory of compartmental dynamical systems. *Journal of Advances in Modeling Earth Systems*, *10*(8), 1729–1734. https://doi.org/10.1029/2018MS001360

Smith, K., Reed, S. C., Cleveland, C. C., Ballantyne, A. P., Anderegg, W. R. L., Wieder, W. R., et al. (2016). Large divergence of satellite and Earth system model estimates of global terrestrial CO_2 fertilization. *Nature Climate Change*, *6*(3), 306–310. https://doi.org/10.1038/nclimate2879

Stephenson, N. L., & van Mantgem, P. J. (2005). Forest turnover rates follow global and regional patterns of productivity. *Ecology Letters*, *8*(5), 524–531. https://doi.org/10.1111/j.1461-0248.2005.00746.x

Stocker, B. D., Zscheischler, J., Keenan, T. F., Prentice, I. C., Seneviratne, S. I., & Peñuelas, J. (2019). Drought impacts on terrestrial primary production underestimated by satellite monitoring. *Nature Geoscience*, *12*(4), 264–270. https://doi.org/10.1038/s41561-019-0318-6

Trugman, A. T., Medvigy, D., Mankin, J. S., & Anderegg, W. R. L. (2018). Soil moisture stress as a major driver of carbon cycle uncertainty. *Geophysical Research Letters*, *45*(13), 6495–6503. https://doi.org/10.1029/2018GL078131

Wang, W., Dungan, J., Hashimoto, H., Michaelis, A. R., Milesi, C., Ichii, K., et al. (2011). Diagnosing and assessing uncertainties of terrestrial ecosystem models in a multimodel ensemble experiment: 1. Primary production. *Global Change Biology*, *17*(3), 1350–1366. https://doi.org/10.1111/j.1365-2486.2010.02309.x

Wang, H., Prentice, I. C., Keenan, T. F., Davis, T. W., Wright, I. J., Cornwell, W. K., et al. (2017). Towards a universal model for carbon dioxide uptake by plants. *Nature Plants*, *3*(9), 734–741. https://doi.org/10.1038/s41477-017-0006-8

Wang, J., Sun, J., Xia, J., He, N., Li, M., & Niu, S. (2018). Soil and vegetation carbon turnover times from tropical to boreal forests. *Functional Ecology*, *32*(1), 71–82. https://doi.org/10.1111/1365-2435.12914

Waring, R. H., Landsberg, J. J., & Williams, M. (1998). Net primary production of forests: A constant fraction of gross primary production? *Tree Physiology*, *18*(2), 129–134. https://doi.org/10.1093/treephys/18.2.129

Wen, Y., Liu, X., Pei, F., Li, X., & Du, G. (2018). Non-uniform time-lag effects of terrestrial vegetation responses to asymmetric warming. *Agricultural and Forest Meteorology*, *252*, 130–143.

Wolter, K., & Timlin, M. S. (2011). El Niño/Southern oscillation behaviour since 1871 as diagnosed in an extended multivariate ENSO index (MEI.ext). *International Journal of Climatology*, *31*(7), 1074–1087. https://doi.org/10.1002/joc.2336

Wu, D., Piao, S., Liu, Y., Ciais, P., & Yao, Y. (2018). Evaluation of CMIP5 Earth system models for the spatial patterns of biomass and soil carbon turnover times and their linkage with climate. *Journal of Climate*, *31*(15), 5947–5960. https://doi.org/10.1175/JCLI-D-17-0380.1

Xia, J., Luo, Y., Wang, Y., & Hararuk, O. (2013). Traceable components of terrestrial carbon storage capacity in biogeochemical models. *Global Change Biology*, *19*(7), 2104–2116. https://doi.org/10.1111/gcb.12172

Yang, Y., Saatchi, S. S., Xu, L., Yu, Y., Choi, S., Phillips, N., et al. (2018). Post-drought decline of the Amazon carbon sink. *Nature Communications*, *9*(1), 1–9. https://doi.org/10.1038/s41467-018-05668-6

Zhang, X., Wang, Y., Peng, S., Rayner, P. J., Ciais, P., Silver, J. D., et al. (2018). Dominant regions and drivers of the variability of the global land carbon sink across timescales. *Global Change Biology*, *24*(9), 3954–3968. https://doi.org/10.1111/gcb.14275

Zhao, M., Heinsch, F. A., Nemani, R. R., & Running, S. W. (2005). Improvements of the MODIS terrestrial gross and net primary production global data set. *Remote Sensing of Environment*, *95*(2), 164–176. https://doi.org/10.1016/j.rse.2004.12.011

Zhao, M., & Running, S. W. (2010). Drought-induced reduction in global terrestrial net primary production from 2000 through 2009. *Science*, *329*(5994), 940–943. https://doi.org/10.1126/science.1192666

Zhao, M., Running, S. W. (2011). Response to comments on "drought-induced reduction in global terrestrial net primary production from 2000 through 2009". *Science*, *333*(6046), 1093. https://doi.org/10.1126/science.1199169

Zhou, S., Liang, J., Luc, X., Lid, Q., Jiang, L., Zhang, Y., et al. (2018). Sources of uncertainty in modeled land carbon storage within and across three MIPs: Diagnosis with three new techniques. *Journal of Climate*, *31*(7), 2833–2851. https://doi.org/10.1175/JCLI

Zhou, S., Zhang, Y., Park Williams, A., & Gentine, P. (2019). Projected increases in intensity, frequency, and terrestrial carbon costs of compound drought and aridity events. *Science advances*, *5*(1), u5740. https://doi.org/10.1126/sciadv.aau5740

Zhu, Z., Bi, J., Pan, Y., Ganguly, S., Anav, A., Xu, L., et al. (2013). Global Data Sets of Vegetation Leaf Area Index (LAI)3g and Fraction of Photosynthetically Active Radiation (FPAR)3g Derived from Global Inventory Modeling and Mapping Studies (GIMMS) Normalized Difference Vegetation Index (NDVI3g) for the Period 1981 to 2011. *Remote Sensing*, *5*(2), 927–948. https://doi.org/10.3390/rs5020927